ACS APPLIED MATERIALS & INTERFACES

Research Article

www.acsami.org

Highly Sensitive and Synergistic Detection of Guanine and Adenine Based on Poly(xanthurenic acid)-Reduced Graphene Oxide Interface

Tao Yang,* Qianqian Kong, Qianhe Li, Xinxing Wang, Lihua Chen, and Kui Jiao

Key Laboratory of Sensor Analysis of Tumor Marker of Education Ministry, College of Chemistry and Molecular Engineering, Qingdao University of Science and Technology, Qingdao 266042, P. R. China

Supporting Information

ABSTRACT: In order to achieve the large direct electrochemical signals of guanine and adenine, an urgent request to explore novel electrode materials and interfaces has been put forward. In this paper, a poly(xanthurenic acid, Xa)-reduced graphene oxide (PXa-ERGNO) interface, which has rich negatively charged active sites and accelerated electron transfer ability, was fabricated for monitoring the positively charged guanine and adenine. Scanning electron microscopy, Fourier transform infrared spectroscopy, Raman spectra, X-ray photoelectron spectroscopy, cyclic voltammetry, electrochemical impedance spectroscopy, and differential pulse voltammetry were adopted to characterize the morphology and prove the electrochemical properties of the prepared interface. The PXa-ERGNO interface with rich negative charge and large electrode surface area was an excellent sensing platform to prompt the adsorption of the positively charged guanine and adenine via strong $\pi-\pi^*$ interaction or electrostatic adsorption. The PXa-ERGNO interface exhibited prominent synergistic effect and good electrocatalytic activity for sensitive determination of guanine and adenine compared with sole PXa or ERGNO modified electrode. The sensing platform we built could be further applied in the adsorption and detection of other positively charged biomolecules or aromatic molecules.

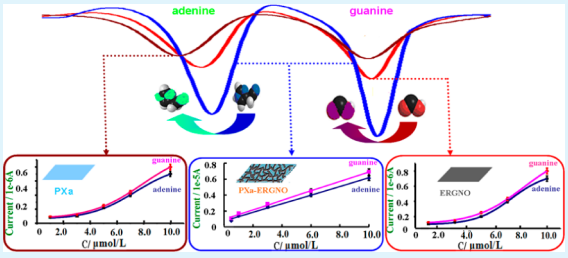

KEYWORDS: *graphene oxide, xanthurenic acid, simultaneous detection, synergistic effect, guanine, adenine*

INTRODUCTION

Since the first report about graphene existing alone (a two-dimensional structure of carbon atoms in crystal with one atom thickness) in 2004,[1] graphene has attracted widespread attention in the electrochemical biosensing field due to its high conductivity, good electrocatalytic activity, and large specific surface area, which have been regarded as the key factors for preparation of electrochemical biosensor.[2] Some graphene types including graphene and functional graphene have been adopted to detect a series of bioactive molecules, such as ascorbic acid, dopamine, paracetamol, and serotonin.[3−5] In DNA sensing field (a key branch of biosensors), various graphene-based materials including sole graphene or graphene nanocomposites (integrated with other functional materials) played more and more important roles not only in DNA hybridization detection but also in the direct electrochemistry of bases.[6−11] For example, a sensitive and selective DNA hybridization assay was developed based on the integration of graphene and polyaniline nanolayers showing high conductivity and good biocompatibility.[12]

Besides being above DNA sequence detection, due to guanine and adenine bases existing inside the dsDNA helix, their direct electrochemical signals on the bare electrode are weak to catch. The exploration of highly sensitive monitors and electrocatalysts is very exigent. Up to now, there have been many reports in the literature on graphene materials or graphene-based nanocomposites as novel sensing platforms to simultaneously detect guanine and adenine.[13−18] Fan et al. fabricated a TiO_2-graphene nanocomposite for the electrochemical detection of guanine and adenine, illustrating the synergistic effect of TiO_2 and graphene could dramatically improve the electrocatalytic activity toward the bases comparing with the sole graphene film.[19] It should be noted that the polymer-based composite films own rich electrochemically active functional groups and excellent redox response, which allows them to serve as synergistic scaffolds for constructing graphene nanocomposites. For instance, a novel biosensor based on electrochemical polymerization of alizarin red (PAR)/graphene composite film was applied to the simultaneous detection of bases, where the high electron transfer ability of PAR is combined with the unique electronic structure of graphene. The nanocomposite with more active sites and accelerated electron transfer rate displayed amazing electrocatalytic properties.[20] Li et al. constructed an electrochemical sensor based on the poly(2,6-pyridinedicarboxylic acid)/chemically reduced graphene oxide composite, which can also exhibit prominent synergistic effects for the simultaneous determination of guanine and adenine.[21]

In this paper, xanthurenic acid (Xa, a nontoxic and excellent redox monomer even in neutral conditions)[22] was integrated

Received: October 4, 2013
Accepted: June 26, 2014
Published: June 26, 2014

   dx.doi.org/10.1021/am502598k | ACS Appl. Mater. Interfaces 2014, 6, 11032−11037

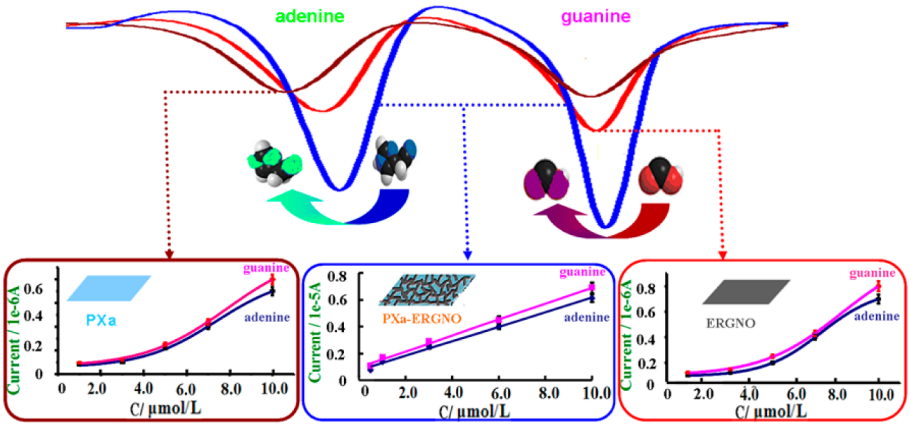

Figure 1. Schematic representation of synergistic detection of guanine and adenine based on PXa-ERGNO.

with graphene oxide (GNO) to construct a negatively charged and specifically structured interface, which can prompt the adsorption of the positively charged guanine and adenine via strong $\pi-\pi^*$ interactions or electrostatic adsorption. The obtained poly(xanthurenic acid)-reduced graphene oxide (PXa-ERGNO) nanocomposite integrating the unique electronic structure and rich active sites of PXa and the high electron transfer ability of ERGNO showed synergistic effects for simultaneous electrocatalytic detection of guanine and adenine (Figure 1).

EXPERIMENTAL SECTION

Chemicals and Apparatus. A CHI 660D electrochemical analyzer (Shanghai CH Instrument Company, China) was used in all of the electrochemical measurements, containing a glassy carbon (GCE) or modified electrode as working electrode, a saturated calomel as reference electrode (SCE), and a platinum wire as counter electrode. Scanning electron microscopy (SEM) measurements were carried out via a JSM-6700F scanning electron microscope (Japan Electron Company). Fourier Transform infrared spectroscopy (FT-IR) spectrum was obtained from Tensor 27 FT-IR spectrophotometer (Bruker Company, German). X-ray photoelectron spectroscopy (XPS) was performed on a Shimadzu ESCA 3600 system with an Mg Kα (1253.6 eV) source and the bonding energy (84.0 eV) of Au 4f as calibration. The Raman spectra was acquired using a Renishaw InVia Raman microscope system with the laser operating at a wavelength of λ = 514 nm with 20 mW laser output power, 30 s collection time, and a 50× magnification objective lens.

Natural graphite (spectral pure, about 30 μm) and Xa were provided by Sinopharm Chemical Reagent Co., Ltd. and Acros Organics (Belgium), respectively. Guanine was acquired from Sigma (St. Louis, MO, USA) and adenine was obtained from BioDee BioTech Co. Ltd. (Beijing, China). All aqueous solutions were prepared with ultrapure water (Aquaplus AWL-1002-P, Ever Young Enterprises Development Co., Ltd., China).

Guanine and adenine storage solutions were dissolved into 0.1 mol/L NaOH solution and kept in a refrigerator at 4 °C. Phosphate buffer solution (PBS) was prepared by mixing the stock solutions of 0.1 mol/L NaH_2PO_4 and 0.1 mol/L Na_2HPO_4. Britton Robinson (BR) buffer solution was obtained by mixing solutions of 0.1 mol/L H_3PO_4, 0.1 mol/L CH_3COOH, and 0.2 mol/L H_3BO_3, and the pH value was adjusted by a certain concentration of NaOH solution.

Fabrication of Various Electrodes. Graphite oxide (GO) was synthesized from graphite powder by a modified Hummers method as originally presented by Hummers.[23] GNO was obtained after suspending the resulting GO in water and sonicating it for 30 min.[24]

The GCE was sequentially polished with 0.3 and 0.05 μm alumina powder and then washed ultrasonically in water and ethanol for a few minutes, and GNO modified electrode was prepared by casting 10 μL of GNO suspension (0.1 mg/mL) on GCE surface to obtain the GNO/GCE.

The electropolymerization of Xa was accomplished by cyclic voltammetry (CV) between 0.65 V and −1.7 V with a scan rate of 100 mV/s at GNO/GCE for 90 segments in fresh PBS (pH 5.5) containing 4×10^{-4} mol/L Xa (SI Figure S1). The resulting electrode was noted as the PXa-ERGNO/GCE. For comparison, the electropolymerization of Xa was accomplished with CV range between 0.65 V and −0.6 V, and the electrochemical reduction of GNO via CV with a potential range from −0.2 V to −1.7 V using bare GCE as working electrode just without GNO or Xa existing to gain the PXa/GCE and ERGNO/GCE.

Electrochemical Measurements. Electrochemical impedance spectroscopy (EIS): the experiment was measured at 0.172 V from 10^5 Hz to 0.1 Hz. The supporting electrolyte was 1.0 mmol/L $K_3Fe(CN)_6$ and 1.0 mmol/L $K_4Fe(CN)_6$ solutions (1:1) including 0.1 mol/L NaCl. CV measurements were carried out in above solution between −0.3 and 0.6 V at a scan rate of 0.1 V/s.

Differential pulse voltammetry (DPV): pulse period, 0.5 s; pulse width, 0.2 s; increment potential, 0.004 V; pulse amplitude, 0.05 V. Unless otherwise stated, BR (pH 7.0) was used as the supporting electrolyte including a certain analytical target for DPV.

Three parallel measurements were measured for each electrode in the same condition in this assay.

RESULTS AND DISCUSSION

Raman, SEM, XPS, and FT-IR Characterization. To characterize the structures of GNO, Raman spectroscopy was adopted (SI Figure S2).[25−29] The two peaks at 1348.6 and 1594.4 cm^{-1} belonged to the D and G bands of GNO, respectively. The D + G bands and 2D band appearing at 2943 and 2694 cm^{-1} also show the existence of GNO. The occurrence and the shape of the 2D band further verified the single-layer structure of the fabricated GNO.[30]

The SEM image of GNO is shown in Figure 2A. The obtained GNO showed slight wrinkles and rough surface. ERGNO (Figure 2B) revealed a more ruffly structure after reduction. The resemblance of crumpled silk veil waves was intrinsic to graphene nanosheets. A protruding and irregular polymer film could be achieved when Xa was electropolymerized alone (Figure 2C). Compared with GNO and PXa, the PXa-ERGNO nanocomposite (Figure 2D) showed a sleek and broad surface after one-step electrochemical synthesis. The change of morphology proved PXa-ERGNO composite film was synthesized successfully.

To show the change of oxygen-containing functional groups attached to the GNO, the XPS for GNO and PXa-ERGNO were investigated (Figure 3).[31−33] The C 1s XPS data of GNO

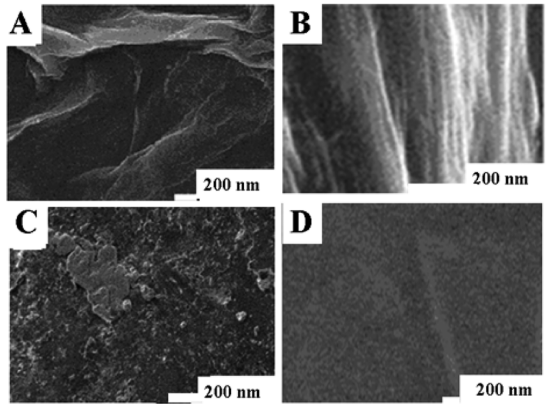

Figure 2. SEM images of GNO (A), ERGNO (B), PXa (C), and PXa-ERGNO (D).

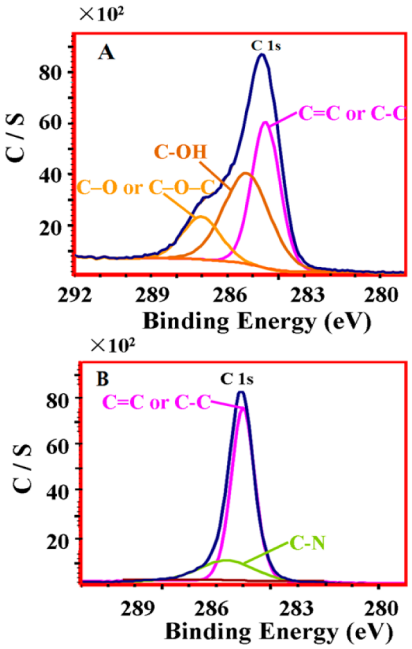

Figure 3. XPS data of GNO (A) and PXa-ERGNO (B).

(Figure 3A) indicated the presence of 3 types of carbon bonds: nonoxygenated C (C═C, C—C, 284.6 eV), C—OH (285.6, eV), C—O, or C—O—C (286.7 eV).[34,35] However, after electrochemical reduction, the peak associated with C—C or C═C became predominant (Figure 3B), while the peaks related to the oxidized carbon species were greatly weakened. In addition, the main peak at the binding energy of 285.6 eV appeared, which confirmed the C—N bonds from PXa.[36−38]

The oxygenated groups could also been confirmed by the FT-IR spectra of GNO (Figure 4A) and PXa-ERGNO (Figure 4B). The typical peaks of GNO appeared at 1065 cm^{-1}(C—O, epoxy or alkoxy), 1401 cm^{-1} (O—H), 1633 cm^{-1} (C═C), and 1740 cm^{-1} (C═O in carboxylic acid and carbonyl moieties). The peak at 3437 cm^{-1} (O—H) could be ascribed to the stretching mode of intercalated water. The above spectra showing the existence of the main functional groups had changed when the GNO was electrochemically reduced. In Figure 4B (PXa-ERGNO), the disappearance of O—H (1401 cm^{-1}) and C═O (1740 cm^{-1}) vibration bands and the maintenance of the O—H stretching vibration (3437 cm^{-1}) and the aromatic C═C (1633 cm^{-1}) demonstrated that the

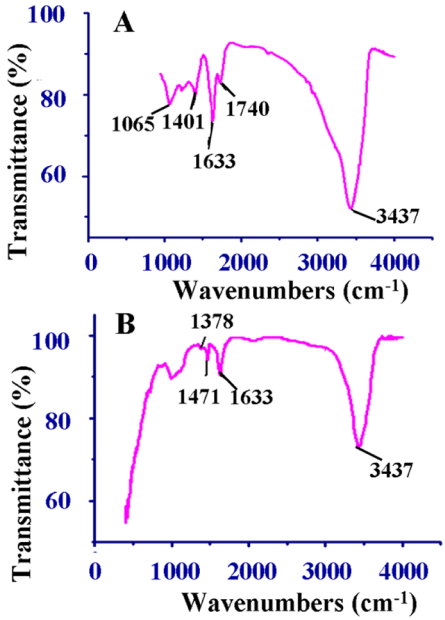

Figure 4. FT-IR data of GNO (A) and PXa-ERGNO (B).

oxygenated species of GNO could be removed by using electrosynthesis.[39] Meanwhile, the bands at 1471 and 1378 cm^{-1} confirmed the presence of O—H and C—N of Xa, respectively. It could be seen that Xa and GNO had been integrated effectively on the basis of all of the above peaks.

Synergistic Effect of PXa-ERGNO. Figure 5A displayed the CVs of PXa/GCE (a), ERGNO/GCE (b), and PXa-

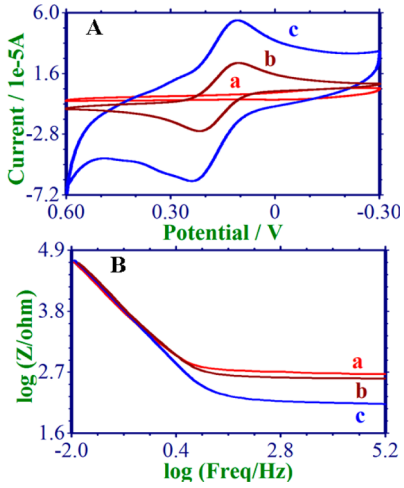

Figure 5. Representative CVs (A) and Bode plots (B) of 1.0 mmol/L $[Fe(CN)_6]^{3-/4-}$ solution containing 0.1 mol/L NaCl recorded at PXa/GCE (a), ERGNO/GCE (b), and PXa-ERGNO/GCE (c).

ERGNO/GCE (c) in 1.0 mmol/L $[Fe(CN)_6]^{3-/4-}$ solution containing 0.1 mol/L NaCl. The redox peak currents of PXa-ERGNO/GCE increase dramatically compared with those of the ERGNO/GCE and PXa/GCE. The result showed that PXa-ERGNO could facilitate the electron transfer of $[Fe(CN)_6]^{3-/4-}$, which was ascribed to the unique synergistic effect of PXa and ERGNO.

EIS was widely applied to research the various surface properties of modified electrodes, normally using $[Fe(CN)_6]^{3-/4-}$ solution containing 0.1 mol/L NaCl as a classic

dx.doi.org/10.1021/am502598k | ACS Appl. Mater. Interfaces 2014, 6, 11032−11037

probe.[17,40] As shown in Figure 5B, logZ of the corresponding Bode plots in the high frequency region was selected for comparison. It could be seen that the logZ value of PXa-ERGNO/GCE (c) was the minimum compared with those of PXa/GCE (a) and ERGNO/GCE (b). This was consistent with the above CV results.

Herein, the electrochemical behavior of 0.3 mmol/L guanine, adenine, and their mixture was investigated at different electrodes in BR (pH 7.0) to examine their bioelectrochemical activity based on the unique synergistic effect of PXa and ERGNO. Figure 6 showed the oxidation signals of bases at

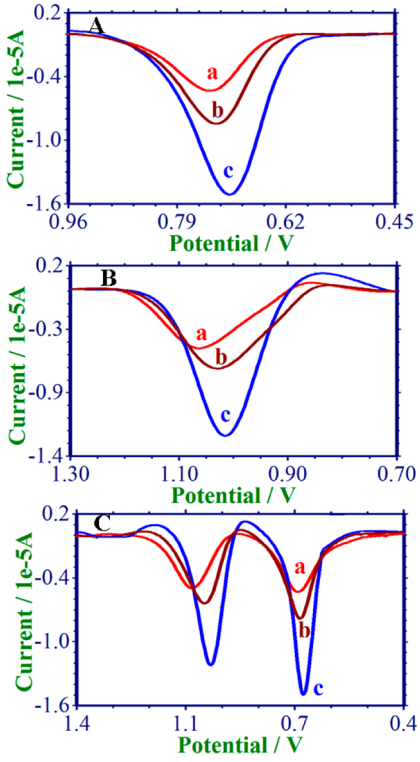

Figure 6. Baseline-corrected DPVs of 0.3 mmol/L guanine (A), adenine (B), and guanine and adenine mixture (C) at different modified electrodes: (a) PXa, (b) ERGNO, and (c) PXa-ERGNO.

PXa/GCE (a), ERGNO/GCE (b), and PXa-ERGNO/GCE (c), and we could see that PXa-ERGNO/GCE exhibited the largest peak currents. It means that PXa-ERGNO prompted the efficiency of the electron exchange between the bases and the electrode surface because of the strong $\pi-\pi^*$ interactions or electrostatic adsorption, and the peak-to-peak separation for guanine and adenine was large enough (Figure 6 C, about 0.3 V) for the simultaneous determination.

Optimization of Preparation Methods and Detection Conditions. The electrochemical detection of bases can be obviously affected by the electrochemical preparation parameters of the PXa-ERGNO/GCE, such as the electropolymerization segments. From SI Figure S3, the maximum current responses of adenine were obtained at 90 segments. Therefore, the electropolymerization segment of 90 was chosen for the subsequent analytical experiments.

The effect of pH values of the detecting electrolyte on the electrooxidation of bases was also studied, as shown in SI Figure S4. The result stated that the oxidation peak potentials of base shifted negatively with the increase of the solution pH from 5.0 to 8.0. The maximum electrooxidation current signal of adenine was observed at pH 7.0, which was selected as the optimization pH.

Individual Detections of Guanine and Adenine. DPV was used to detect individual guanine and adenine with a series of concentrations (low and high concentration section) under optimal conditions. It is shown in Figure 7A that two linear

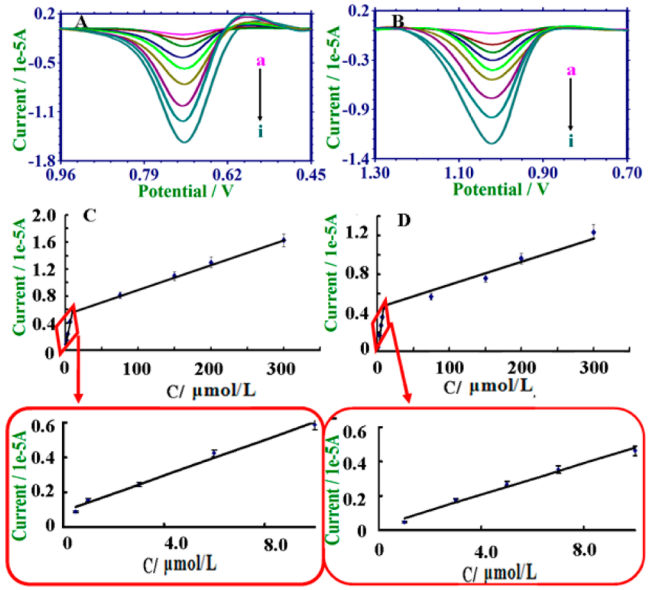

Figure 7. (A) Baseline-corrected DPVs of various guanine concentrations at PXa-ERGNO/GCE (from a to i: 0.5, 1, 3, 6, 10, 75, 150, 200, 300 μmol/L). (B) Baseline-corrected DPVs of various adenine concentrations at PXa-ERGNO/GCE (from a to i: 1, 3, 5, 7, 10, 75, 150, 200, 300 μmol/L). (C) Calibration plots of the oxidation peak current versus different concentrations of guanine. (D) Calibration plots of the oxidation peak current versus different concentrations of adenine.

regions were observed in the calibration curve of guanine,[19] I = 0.0701C + 0.1442 (r = 0.9688) (0.5 μmol/L to 10 μmol/L) and I = 0.0027C + 0.8459 (r = 0.9722) (10 μmol/L to 300 μmol/L). The detection limit (S/N = 3) was 0.032 μmol/L (Figure 7C).

Studies similar to those with adenine were carried out and the calibration curves revealed the same trend from 1 μmol/L to 300 μmol/L (Figure 7B). The linear regression equation was I = 0.0577C − 0.0034 (r = 0.9787) (1 μmol/L to 10 μmol/L) and I = 0.0023C + 0.5762 (r = 0.9853) (10 μmol/L to 300 μmol/L). The detection limit (S/N = 3) was 0.15 μmol/L (Figure 7D).

Comparison of Simultaneous Detection of Guanine and Adenine. In order to investigate if the PXa-ERGNO/GCE had the best sensitivity, comparison of the electrochemical simultaneous detection of guanine and adenine mixture at PXa/GCE, ERGNO/GCE, and PXa-ERGNO/GCE was carried out, shown in Figure 8. The PXa-ERGNO had the highest electrochemical response, lowest detection limit, and good linear relation. At PXa-ERGNO/GCE, the calibration curves for guanine and adenine exhibited two linear segments with regression equation as I = 0.0793C + 0.1514 (r = 0.9862) (0.5 μmol/L to 10 μmol/L); I = 0.0024C + 0.8948 (r = 0.9869) (10 μmol/L to 300 μmol/L) for guanine; and I = 0.076C + 0.1054 (r = 0.9876) (0.5 μmol/L to 10 μmol/L) and I = 0.002C + 0.8195 (r = 0.9889) (10 μmol/L to 300 μmol/L)

dx.doi.org/10.1021/am502598k | ACS Appl. Mater. Interfaces 2014, 6, 11032−11037

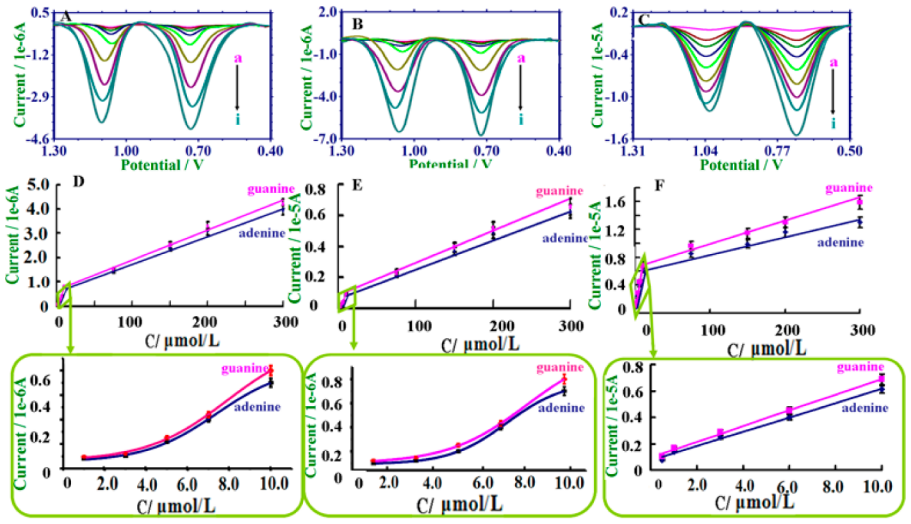

Figure 8. Baseline-corrected DPVs of various guanine and adenine concentrations at (A) PXa/GCE (from a to i: 1 to 300 μmol/L), (B) ERGNO/GCE (from a to i: 1 to 300 μmol/L), and (C) PXa-ERGNO/GCE (from a to i: 0.5 to 300 μmol/L). Calibration plots of the oxidation peak current versus different concentrations of guanine and adenine concentrations at PXa/GCE (D), ERGNO/GCE (E), and PXa-ERGNO/GCE (F).

for adenine. Therefore, the guanine and adenine could be sensitively and simultaneously determined from a mixture in a large concentration domain.

Reproducibility and Stability of the Modified Electrode. Ten modified electrodes obtained from the same procedure were used to detect 0.3 mmol/L guanine and 0.3 mmol/L adenine to estimate the reproducibility. The relative standard deviation (RSD) for the oxidation peak current of guanine and adenine are, respectively, 6.5% and 6.2%, showing the good reproducibility of the fabrication protocol.

The stability of guanine and adenine on the modified surface is an important factor, which plays a critical role for obtaining good sensitivity. It showed the long-term stability by keeping the modified electrodes at room temperature for 5 days. During that time, the modified electrodes could still detect guanine and adenine in the same concentration solution, and 3.7% loss for guanine and 3.9% loss for adenine of the peak currents were observed. The results demonstrated that the detection signals had no obvious decline.

Comparsion of Our Work and Previous Reports. Our assay was also compared with previous reports: please see Supporting Information. As can be seen from Table S3, our work possessed the advantages of easier preparation, controlled synthesis, and wider linear range as compared with other earlier reports.

CONCLUSION

In summary, compared with the sole PXa or ERGNO, the PXa-ERGNO interface had lower overpotentials and higher peak currents, exhibiting a remarkable synergistic effect for the oxidation of guanine and adenine. That is to say that the nanocomposite could greatly accelerate the electron exchange between bases and electrode, and further promote the oxidation property of bases on electrode surface. Moreover, our PXa-ERGNO/GCE with rich negative charge and large electrode surface area is easy to prepare. This easy to prepare, nontoxic, and excellent sensing platform can improve the adsorption of other positively charged biomolecules or aromatic molecules via strong electrostatic adsorption or $\pi-\pi^*$ interactions, which can be further used in biological and medical applications.

ASSOCIATED CONTENT

Supporting Information

Electrochemical process of PXa, Raman spectra of GNO, optimization of preparation methods and detection conditions, and the comparison of our works and previous reports, as noted in text. This material is available free of charge via the Internet at http://pubs.acs.org.

AUTHOR INFORMATION

Corresponding Author

*Phone: +86-532-84022665. Fax: +86-532-84023927. E-mail: taoyang@qust.edu.cn.

Notes

The authors declare no competing financial interest.

ACKNOWLEDGMENTS

This work was supported by the National Natural Science Foundation of China (No. 21275084, 20975057), Doctoral Foundation of the Ministry of Education of China (No. 20113719130001), 863 program (No. 2013AA032204), Scientific and Technical Development Project of Qingdao (No. 12-1-4-3-(23)-jch), and Outstanding Adult-Young Scientific Research Encouraging Foundation of Shandong Province (No. BS2012CL013).

REFERENCES

(1) Novoselov, K. S.; Geim, A. K.; Morozov, S. V.; Jiang, D.; Zhang, Y.; Dubonos, S. V.; Grigorieva, I. V.; Firsov, A. A. Electric Field Effect in Atomically Thin Carbon Films. *Science* **2004**, *306*, 666−669.

(2) Shao, Y. Y.; Wang, J.; Wu, H.; Liu, J.; Aksay, I. A.; Lin, Y. H. Graphene Based Electrochemical Sensors and Biosensors: A Review. *Electroanalysis* **2010**, *22*, 1027−1036.

(3) Kim, Y. R.; Bong, S.; Kang, Y. J.; Yang, Y.; Mahajan, R. K.; Kim, J. S.; Kim, H. Electrochemical Detection of Dopamine in the Presence of Ascorbic Acid Using Graphene Modified Electrodes. *Biosens. Bioelectron.* **2010**, *25*, 2366−2369.

(4) Alwarappan, S.; Erdem, A.; Liu, C.; Li, C. Z. Probing the Electrochemical Properties of Graphene Nanosheets for Biosensing Applications. *J. Phys. Chem. C* **2009**, *113*, 8853−8857.

(5) Kang, X. H.; Wang, J.; Wu, H.; Liu, J.; Aksay, I. A.; Lin, Y. H. A Graphene-Based Electrochemical Sensor for Sensitive Detection of Paracetamol. *Talanta* **2010**, *81*, 754−759.
(6) Bonanni, A.; Pumera, M. Graphene Platform for Hairpin-DNA-Based Impedimetric Genosensing. *ACS Nano* **2011**, *5*, 2356−2361.
(7) Muti, M.; Sharma, S.; Erdem, A.; Papakonstantinou, P. Electrochemical Monitoring of Nucleic Acid Hybridization by Single-Use Graphene Oxide-Based Sensor. *Electroanalysis* **2011**, *23*, 272−279.
(8) Erdem, A.; Muti, M.; Papakonstantinou, P.; Canavar, E.; Karadeniz, H.; Congur, G.; Surbhi, S. Graphene Oxide Integrated Sensor for Electrochemical Monitoring of Mitomycin C-DNA Interaction. *Analyst* **2012**, *137*, 2129−2135.
(9) Liu, Y. X.; Dong, X. C.; Chen, P. Biological and Chemical Sensors Based on Graphene Materials. *Chem. Soc. Rev.* **2012**, *41*, 2283−2307.
(10) Yang, T.; Guan, Q.; Guo, X. H.; Meng, L.; Du, M.; Jiao, K. Direct and Freely Switchable Detection of Target Genes Engineered by Reduced Graphene Oxide-Poly(*m*-aminobenzenesulfonic acid) Nanocomposite via Synchronous Pulse-Electrosynthesis. *Anal. Chem.* **2013**, *85*, 1358−1366.
(11) Yang, T.; Meng, L.; Wang, X. X.; Wang, L. L.; Jiao, K. Direct Electrochemical DNA Detection Based on the Self-Redox Signal of Sulfonated Polyaniline Enhanced by Graphene Oxide in Neutral Solution. *ACS Appl. Mater. Interfaces* **2013**, *5*, 10889−10894.
(12) Bo, Y.; Yang, H. Y.; Hu, Y.; Yao, T. M.; Huang, S. S. A Novel Electrochemical DNA Biosensor Based on Graphene and Polyaniline Nanowires. *Electrochim. Acta* **2011**, *56*, 2676−2681.
(13) Akhavan, O.; Ghaderi, E.; Rahighi, R. Toward Single-DNA Electrochemical Biosensing by Graphene Nanowalls. *ACS Nano* **2012**, *6*, 2904−2916.
(14) Lim, C. X.; Hoh, H. Y.; Ang, P. K.; Loh, K. P. Direct Voltammetric Detection of DNA and pH Sensing on Epitaxial Graphene: An Insight into the Role of Oxygenated Defects. *Anal. Chem.* **2010**, *82*, 7387−7393.
(15) Yang, T.; Guan, Q.; Li, Q. H.; Meng, L.; Wang, L. L.; Liu, C. X.; Jiao, K. Large-Area, Three-Dimensional Interconnected Graphene Oxide Intercalated with Self-Doped Polyaniline Nanofibers as a Free-Standing Electrocatalytic Platform for Adenine and Guanine. *J. Mater. Chem. B* **2013**, *1*, 2926−2933.
(16) Zhu, X. H.; Zeng, L. X.; Xu, M. T.; Liang, Y.; Nan, J. M. A Glassy Carbon Electrode Modified with Electrochemically Reduced Graphene for Simultaneous Determination of Guanine and Adenine. *Anal. Methods* **2012**, *4*, 2935−2939.
(17) Niu, X. L.; Yang, W.; Ren, J.; Guo, H.; Long, S. J.; Chen, J. J.; Gao, J. Z. Electrochemical Behaviors and Simultaneous Determination of Guanine and Adenine Based on Graphene-Ionic Liquid-Chitosan Composite Film Modified Glassy Carbon Electrode. *Electrochim. Acta* **2012**, *80*, 346−353.
(18) Yin, H. S.; Zhou, Y. L.; Ma, Q.; Ai, S. Y.; Ju, P.; Zhu, L. S.; Lu, L. N. Electrochemical Oxidation Behavior of Guanine and Adenine on Graphene-Nafion Composite Film Modified Glassy Carbon Electrode and the Simultaneous Determination. *Process Biochem.* **2010**, *45*, 1707−1712.
(19) Fan, Y.; Huang, K. J.; Niu, D. J.; Yang, C. P.; Jing, Q. S. TiO_2-Graphene Nanocomposite for Electrochemical Sensing of Adenine and Guanine. *Electrochim. Acta* **2011**, *56*, 4685−4690.
(20) Ba, X.; Luo, L. Q.; Ding, Y. P.; Zhang, Z.; Chu, Y. L.; Wang, B. J.; Ouyang, X. Q. Poly(alizarin red)/Graphene Modified Glassy Carbon Electrode for Simultaneous Determination of Purine and Pyrimidine. *Anal. Chim. Acta* **2012**, *752*, 94−100.
(21) Li, C. X.; Qiu, X. Y.; Ling, Y. L. Electrocatalytic Oxidation and the Simultaneous Determination of Guanine and Adenine on (2,6-pyridinedicarboxylic acid)/Graphene Composite Film Modified Electrode. *J. Electroanal. Chem.* **2013**, *704*, 44−49.
(22) Yang, T.; Li, X.; Li, Q. H.; Guo, X. H.; Guan, Q.; Jiao, K. Electrochemically Reduced Graphene Oxide-Enhanced Electropolymerization of Poly-Xanthurenic Acid for Direct, "Signal-on" and High Sensitive Impedimetric Sensing of DNA. *Polym. Chem.* **2013**, *4*, 1228−1234.
(23) Hummers, W. S.; Offeman, R. E. Preparation of Graphitic Oxide. *J. Am. Chem. Soc.* **1958**, *80*, 1339−1339.
(24) Yang, T.; Li, Q. H.; Li, X.; Wang, X. H.; Du, M.; Jiao, K. Freely Switchable Impedimetric Detection of Target Gene Sequence Based on Synergistic Effect of ERGNO/PANI Nanocomposites. *Biosens. Bioelectron.* **2013**, *42*, 415−418.
(25) Calizo, I.; Balandin, A. A.; Bao, W.; Miao, F.; Lau, C. N. Temperature Dependence of the Raman Spectra of Graphene and Graphene Multilayers. *Nano Lett.* **2007**, *7*, 2645−2649.
(26) Kudin, K. N.; Ozbas, B.; Schniepp, H. C.; Prud'homme, R. K.; Aksay, I. A.; Car, R. Raman Spectra of Graphite Oxide and Functionalized Graphene Sheets. *Nano Lett.* **2008**, *8*, 36−41.
(27) Kim, K. S.; Zhao, Y.; Jang, H.; Lee, S. Y.; Kim, J. Min.; Kim, K. S.; Ahn, J. H.; Kim, P.; Choi, J. Y.; Hong, B. H. Large-Scale Pattern Growth of Graphene Films for Stretchable Transparent Electrodes. *Nature* **2009**, *457*, 706−710.
(28) Ferrari, A. C.; Meyer, J. C.; Scardaci, V.; Casiraghi, C.; Lazzeri, M.; Mauri, F.; Piscanec, S.; Jiang, D.; Novoselov, K. S.; Roth, S.; Geim, A. K. Raman Spectrum of Graphene and Graphene Layers. *Phys. Rev. Lett.* **2006**, *97*, 187401−187404.
(29) Akhavan, O.; Ghaderi, E. Graphene Nanomesh Promises Extremely Efficient in Vivo Photothermal Therapy. *Small* **2013**, *9*, 3593−3601.
(30) Yang, T.; Guo, X. H.; Kong, Q. Q.; Li, Q. H.; Jiao, K. Comparative Studies on Zirconia and Graphene Composites Obtained by One-Step and Stepwise Electrodeposition for Deoxyribonucleic Acid Sensing. *Anal. Chim. Acta* **2013**, *786*, 29−33.
(31) Caro, B. A. M.; Armini, S.; Richard, O.; Maes, G.; Borghs, G.; Whelan, C. M.; Travaly, Y. Bottom-Up Engineering of Subnanometer Copper Diffusion Barriers Using NH_2-Derived Self-Assembled Monolayers. *Adv. Funct. Mater.* **2010**, *20*, 1−7.
(32) Akhavan, O.; Kalaee, M.; Alavi, Z. S.; Ghiasi, S. M. A.; Esfandiar, A. Increasing the Antioxidant Activity of Green Tea Polyphenols in the Presence of Iron for the Reduction of Graphene Oxide. *Carbon* **2012**, *50*, 3015−3025.
(33) Bai, H.; Xu, Y. X.; Zhao, L.; Li, C.; Shi, G. Q. Non-Covalent Functionalization of Graphene Sheets by Sulfonated Polyaniline. *Chem. Commun.* **2009**, *13*, 1667−1669.
(34) Chen, W. F.; Yan, L. F. In Situ Self-Assembly of Mild Chemical Reduction Graphene for Three-Dimensional Architectures. *Nanoscale* **2011**, *3*, 3132−3137.
(35) Chandra, V.; Park, J.; Chun, Y.; Lee, J. W.; Hwang, I. C.; Kim, K. S. Water-Dispersible Magnetite-Reduced Graphene Oxide Composites for Arsenic Removal. *ACS Nano* **2010**, *4*, 3979−3986.
(36) Akhavan, O.; Ghaderi, E. Toxicity of Graphene and Graphene Oxide Nanowalls Against Bacteria. *ACS Nano* **2010**, *4*, 5731−5736.
(37) Zhang, J.; Lei, J. P.; Pan, R.; Xue, Y. D.; Ju, H. X. Highly Sensitive Electrocatalytic Biosensing of Hypoxanthine Based on Functionalization of Graphene Sheets with Water-Soluble Conducting Graft Copolymer. *Biosens. Bioelectron.* **2010**, *26*, 371−376.
(38) Yang, T.; Li, Q. H.; Meng, L.; Wang, X. H.; Chen, W. W.; Jiao, K. Synchronous Electrosynthesis of Poly(xanthurenic acid)-Reduced Graphene Oxide Nanocomposite for Highly Sensitive Impedimetric Detection of DNA. *ACS Appl. Mater. Interfaces* **2013**, *5*, 3495−3499.
(39) Du, M.; Yang, T.; Jiao, K. Immobilization-Free Direct Electrochemical Detection for DNA Specific Sequences Based on Electrochemically Converted Gold Nanoparticles/Graphene Composite Film. *J. Mater. Chem.* **2010**, *20*, 9253−9260.
(40) Meziane, D.; Barras, A.; Kromka, A.; Houdkova, J.; Boukherroub, R.; Szunerits, S. Thiol-Yne Reaction on Boron-Doped Diamond Electrodes: Application for the Electrochemical Detection of DNA-DNA Hybridization Events. *Anal. Chem.* **2012**, *84*, 194−200.